

# Extended GeV-TeV Emission around a Gamma-Ray Burst Remnant: The case of W49B

Kunihiro Ioka<sup>1</sup>, Shiho Kobayashi<sup>1,2</sup>, and Peter Mészáros<sup>1,2,3</sup>

<sup>1</sup>*Physics Department and Center for Gravitational Wave Physics, 104 Davey Laboratory, Pennsylvania State University, University Park, PA 16802*

<sup>2</sup>*Department of Astronomy and Astrophysics, 525 Davey Laboratory, Pennsylvania State University, University Park, PA 16802*

<sup>3</sup>*The Institute for Advanced Study, Einstein Drive, Princeton, NJ 08540*

## ABSTRACT

We consider the recent report that the supernova remnant W49B is a Gamma-Ray Burst (GRB) remnant in our Galaxy. If this is correct, and if GRBs are sources of ultrahigh-energy cosmic rays (UHECRs), a natural consequence of this identification would be a detectable GeV-TeV photon emission around the GRB remnant. The imaging of the surrounding emission could provide new constraints on the jet structure of the GRB.

*Subject headings:* cosmic rays — gamma rays: bursts — gamma rays: theory

## 1. Introduction

Past Gamma-Ray Burst (GRB) occurrences in our galaxy may have left radio remnants resembling hyperenergetic supernovae (e.g., Perna & Loeb 2000). Recently, Chandra X-ray observations have led to infer that the supernova remnant W49B (G43.3-0.2) may be the first remnant of a GRB discovered in the Milky Way (see CXC Press Release: 04-05 in <http://chandra.harvard.edu/>). This remnant is located at  $d \sim 10$  kpc from earth, has a radius of  $R \sim 10$  pc, and is estimated to have occurred  $\sim 3000$  yr ago in our Galaxy.

In this Letter we discuss the high energy implications of the GRB origin of some supernova-like remnants, and in particular of the assumption that W49B is a GRB remnant. We show that, if we also assume that GRBs are sources of ultrahigh-energy cosmic rays (UHECRs), significant GeV-TeV gamma-ray emission may be detectable around W49B. A non-detection may rule out either that W49B is a GRB remnant, or that the GRBs can efficiently accelerate UHECRs.

GRBs are one of the most promising candidates for the origin of UHECRs (Waxman 1995; Vietri 1995; Milgrom & Usov 1995). The physical conditions required in GRBs to produce MeV gamma-rays also allow protons to be accelerated up to  $\sim 10^{20}$  eV. In addition, the energy generation rate of UHECRs in the range  $10^{19}$ - $10^{21}$  eV,  $\dot{\epsilon}_{[10^{19},10^{21}]\text{eV}}^{\text{CR}}$ , is similar to the  $\gamma$ -ray generation rate of GRBs,  $\dot{\epsilon}_{\gamma[0.02,2]\text{MeV}}^{\text{GRB}}$  (Waxman 2004; Vietri, De Marco, & Guetta 2003),

$$\dot{\epsilon}_{[10^{19},10^{21}]\text{eV}}^{\text{CR}} \sim 3\dot{\epsilon}_{\gamma[0.02,2]\text{MeV}}^{\text{GRB}}, \quad (1)$$

suggesting that GRBs are the sources of UHECRs. We note that for the purposes of this Letter, even UHECR of energies well below  $10^{20}$  eV can lead to a GeV-TeV photon emission.

If the GRBs are the origin of UHECRs, an unavoidable component of the UHECR outflow, of comparable energy, is going to be in the form of neutrons. This is because protons are trapped by the magnetic field in the ejecta, being subjected to energy losses due to adiabatic cooling as the ejecta expands (Rachen & Mészáros 1998) and conversion into neutrons via photomeson interactions,  $p\gamma \rightarrow n\pi^+$ , between the accelerated protons and the GRB photons. The optical depth for this process is about a few for protons with energy  $\gtrsim 10^{16}$  eV (Waxman & Bahcall 1997; Vietri 1998). These high energy neutrons decay into protons and electrons outside the ejecta,  $n \rightarrow p + e^- + \bar{\nu}_e$ , followed by the interaction with the surroundings. This results in photon, neutrino and neutron emission around the remnant (Dermer 2002; Biermann, Medina Tanco, Engel, & Pugliese 2004).

In this Letter we consider the photon emission from  $\beta$ -decay electrons and discuss its detectability for the W49B case. We find that the GeV emission may be marginally detected by GLAST. The TeV emission is probably detectable by the future atmospheric Cherenkov telescope VERITAS, while HEGRA may have already detected this signal in their archival data, and we strongly urge the reanalysis of the HEGRA database. The emission from  $\beta$ -decay protons will be discussed in the subsequent paper.

## 2. $\beta$ -decay electron emission around the GRB remnant

Most GRBs have geometrically corrected gamma-ray energies of about  $10^{51}$  erg (Bloom, Frail, & Kulkarni 2003). According to equation (1), GRBs could then emit a comparable energy of  $\sim 10^{51}$  erg in high energy neutrons, with roughly equal energy in each decade of the energy band if the neutron (proton) spectrum has a number spectral index 2. In GRBs such a spectral index  $\sim 2$  is expected above the neutron (proton) energy  $\gtrsim 10^{16}$  eV, and  $\sim 1$  below it (Waxman & Bahcall 1997). Because of the relativistic beaming, the neutrons are also beamed into a jet.

We first consider each decade of neutron energy, to simplify the discussion. We assume that the GRB ejects neutrons with a Lorentz factor  $\gamma_n \sim 10^8 \gamma_{n,8}$  and a total energy  $E_n \sim 10^{51} E_{n,51}$  erg, at a time  $t_{\text{age}} \sim 3000 t_{\text{age},3.5}$  yr ago. These neutrons decay,  $n \rightarrow p + e^- + \bar{\nu}_e$ , over

$$t_{\text{decay}} \sim \gamma_n t_\beta \sim 3 \times 10^3 \gamma_{n,8} \text{ yr}, \quad (2)$$

producing high energy electrons with a Lorentz factor  $\gamma_e \sim \gamma_n$ . Here  $t_\beta \sim 900$  s is the  $\beta$ -decay time in the comoving frame. The energy of the  $\beta$ -decay electrons is  $m_p/m_e \sim 10^3$  times smaller than that of the neutrons. Nevertheless we will concentrate on the emission from these  $\beta$ -decay electrons in this Letter, since electrons radiate more efficiently than protons. We consider only electrons with  $\gamma_e \sim \gamma_n \gtrsim 10^6$ , from neutrons which decay outside the remnant,  $ct_{\text{decay}} \gtrsim R$ , so that we can easily separate the  $\beta$ -decay emission from the remnant emission, such as due to the pion decay (Enomoto et al. 2002).

The  $\beta$ -decay electrons radiate via synchrotron and the inverse Compton (IC) emission. The corresponding fluxes depend on the energy densities of the magnetic and photon fields. We adopt the typical magnetic field in our Galaxy  $B \sim 3 \mu\text{G}$  corresponding to a magnetic energy density  $U_B \sim 4 \times 10^{-13} \text{ erg cm}^{-3}$ . For the IC process, we consider the infrared (IR), optical and cosmic microwave background (CMB) as the main target photons. The energy density of these background photons is about  $U_{\text{IR}} \sim 2 \times 10^{-13} \text{ erg cm}^{-3}$ ,  $U_{\text{opt}} \sim 7 \times 10^{-13} \text{ erg cm}^{-3}$ , and  $U_{\text{CMB}} \sim 4 \times 10^{-13} \text{ erg cm}^{-3}$ , and the typical temperatures are about  $\epsilon_{\text{IR}} \sim 100 \text{ K}$ ,  $\epsilon_{\text{opt}} \sim 6000 \text{ K}$ , and  $\epsilon_{\text{CMB}} \sim 3 \text{ K}$  (e.g., Mathis, Mezger, & Panagia 1983). Then the cooling time of electrons due to all the combined emissions is

$$t_{\text{cool}}(\gamma_e) \sim \frac{3m_e c}{4\gamma_e \sigma_T U_{\text{total}}} \sim 1 \times 10^4 \gamma_{e,8}^{-1} U_{\text{total},-12}^{-1} \text{ yr}, \quad (3)$$

where  $U_{\text{total}} = U_B + \bar{U}_{\text{IR}} + \bar{U}_{\text{opt}} + \bar{U}_{\text{CMB}} = 10^{-12} U_{\text{total},-12} \text{ erg cm}^{-3}$  is the total energy density, and we use  $\bar{U}_\gamma = U_\gamma \min(1, m_e c^2 / \epsilon_\gamma \gamma_e)$  to take the Klein-Nishina (KN) effect into account (where the suffix  $\gamma = \text{IR}$ ,  $\text{opt}$ , or  $\text{CMB}$ ).

There are two cases, depending on whether or not most of the neutrons decay within the remnant age, the latter case being divided into two sub-cases depending on whether or not the electrons cool slower than the remnant age, leading to three different types of emission region shape.

(a) Fast decay,  $t_{\text{decay}}(\gamma_e) < t_{\text{age}}$ : In this case the fraction of neutrons that have decayed is  $f_\beta \sim 1$ . The radius of the emitting region is roughly equal to the  $\beta$ -decay length  $\sim ct_{\text{decay}} \sim 0.9 \gamma_{n,8} \text{ kpc}$ , which is much larger than the Larmor radius of the  $\beta$ -decay electrons,

$$r_L \sim \frac{\gamma_e m_e c^2}{qB} \sim 6 \times 10^{-2} \gamma_{e,8} B_{-6}^{-1} \text{ pc}, \quad (4)$$

where  $B = 10^{-6}B_{-6}$  G. Thus, the sky distribution of the emitting region is roughly preserved, as shown in Figure 1 (a). The emitting region has an elongated shape on the sky, whose solid angle is approximately

$$\Omega \sim 4\theta(ct_{\text{decay}}/d)^2 \sim (1\theta_{-1}\gamma_{e,8})^\circ \times (10\gamma_{e,8})^\circ \sim 3 \times 10^{-3}\theta_{-1}\gamma_{e,8}^2 \text{ sr}, \quad (5)$$

if the opening half-angle of the jet is  $\theta = 0.1\theta_{-1}$ .

An electron with an initial cooling time  $t_{\text{cool}}(\gamma_e) < t_{\text{age}}$  cools down to the Lorentz factor determined by  $t_{\text{cool}}(\gamma_e) \sim t_{\text{age}}$ . Thus the current Lorentz factor of electrons is given by

$$\hat{\gamma}_e \sim \min\left(\gamma_e, \frac{3m_e c}{4t_{\text{age}}\sigma_T U_{\text{total}}}\right) \sim 1 \times 10^8 \min(\gamma_{e,8}, 3t_{\text{age},3.5}^{-1} U_{\text{total},-12}^{-1}). \quad (6)$$

Irrespective of the initial  $\gamma_e$ , the order of magnitude of the current Lorentz factor  $\hat{\gamma}_e$  is the same in all the emitting region, so that the surface brightness on the sky is nearly homogeneous.

The characteristic synchrotron frequency and the synchrotron peak flux at the observer are given by

$$\begin{aligned} \nu_m &= \frac{qB\hat{\gamma}_e^2}{2\pi m_e c} \sim 1 \times 10^2 B_{-6} \hat{\gamma}_{e,8}^2 \text{ eV}, \\ \nu F_\nu(\nu_m) &\sim \frac{m_e \hat{\gamma}_e}{m_p \gamma_e} \frac{U_B}{U_{\text{total}}} \frac{f_\beta E_n}{4\pi d^2 t_{\text{cool}}(\hat{\gamma}_e)} \sim 1 \times 10^{-10} f_\beta E_{n,51} U_{B,-12} \hat{\gamma}_{e,8}^2 \gamma_{e,8}^{-1} \text{ erg s}^{-1} \text{ cm}^{-2}. \end{aligned} \quad (7)$$

Similarly the characteristic IC frequency and the IC peak flux are

$$\begin{aligned} \nu_\gamma &\sim \min(\hat{\gamma}_e m_e c^2, \epsilon_\gamma \hat{\gamma}_e^2) \sim 10 \min(5\hat{\gamma}_{e,8}, \epsilon_{\gamma,-3} \hat{\gamma}_{e,8}^2) \text{ TeV} \\ \nu F_\nu(\nu_\gamma) &\sim \frac{m_e \hat{\gamma}_e}{m_p \gamma_e} \frac{\bar{U}_\gamma}{U_{\text{total}}} \frac{f_\beta E_n}{4\pi d^2 t_{\text{cool}}(\hat{\gamma}_e)} \sim 1 \times 10^{-10} f_\beta E_{n,51} \bar{U}_{\gamma,-12} \hat{\gamma}_{e,8}^2 \gamma_{e,8}^{-1} \text{ erg s}^{-1} \text{ cm}^{-2}, \end{aligned} \quad (8)$$

where  $\epsilon_\gamma = 10^{-3}\epsilon_{\gamma,-3}$  eV is the target photon energy. The surface brightness of emission is about  $S = \nu F_\nu/\Omega \sim 5 \times 10^{-8} \theta_{-1}^{-1} E_{n,51} U_{B,-12} \hat{\gamma}_{e,8}^2 \gamma_{e,8}^{-3}$  erg s<sup>-1</sup> cm<sup>-2</sup> sr<sup>-1</sup>.

(b) Slow decay,  $t_{\text{decay}}(\gamma_e) > t_{\text{age}}$ . In this case, almost all neutrons are still decaying. The radius of the emitting region is roughly  $\sim ct_{\text{age}} \sim 1t_{\text{age},3.5}$  kpc, which is again larger than the Larmor radius in equation (4) for our parameters. In this case, however, the shape of the emitting region depends on whether electrons cool within the remnant age or not.

(b1) If  $t_{\text{cool}}(\gamma_e) > t_{\text{age}}$ , the electrons do not cool much, so the current Lorentz factor of the electrons is  $\hat{\gamma}_e \sim \gamma_e$ . Thus the surface brightness of the emitting region is nearly homogeneous (see Figure 1 (b1)). The fraction of neutrons that have decayed is  $f_\beta \sim t_{\text{age}}/t_{\text{decay}} \sim 1t_{\text{age},3.5} \gamma_{e,8}^{-1}$ . The solid angle of the emitting region on the sky is about

$$\Omega \sim 4\theta(ct_{\text{age}}/d)^2 \sim (1\theta_{-1} t_{\text{age},3.5})^\circ \times (10t_{\text{age},3.5})^\circ \sim 4 \times 10^{-3} \theta_{-1} t_{\text{age},3.5}^2 \text{ sr}. \quad (9)$$

The synchrotron and IC emission is given by equations (7) and (8), respectively. The surface brightness of the emission is  $S = \nu F_\nu / \Omega \sim 4 \times 10^{-8} \theta_{-1}^{-1} E_{n,51} U_{-12} t_{\text{age},3.5}^{-1} \text{ erg s}^{-1} \text{ cm}^{-2} \text{ sr}^{-1}$ .

(b2) If  $t_{\text{cool}}(\gamma_e) < t_{\text{age}}$ , almost all the electrons cool down, except for a smaller fraction of electrons at the jet head which have not cooled yet because the neutrons are just decaying,  $t_{\text{decay}}(\gamma_e) > t_{\text{age}}$ . Although the number of these hot electrons is small, the flux from these hot electrons dominates that of the rest, since they have a larger energy and a shorter cooling time (see Figure 1 (b2)). Thus we concentrate on the hot electrons within the distance  $\sim ct_{\text{cool}}(\gamma_e) \sim 3\gamma_{e,8}^{-1} U_{\text{total},-12}^{-1}$  kpc from the jet head. The current Lorentz factor of these electrons is  $\hat{\gamma}_e \sim \gamma_e$ , and the fraction of neutrons that have decayed is  $f_\beta \sim t_{\text{cool}}/t_{\text{decay}} \sim 3\gamma_{e,8}^{-2} U_{\text{total},-12}^{-1}$ . The solid angle of the emitting region on the sky is

$$\begin{aligned} \Omega &\sim 4\theta(ct_{\text{age}}/d)(ct_{\text{cool}}/d) \sim (1\theta_{-1} t_{\text{age},3.5})^\circ \times (30\gamma_{e,8}^{-1} U_{\text{total},-12}^{-1})^\circ \\ &\sim 1 \times 10^{-2} \theta_{-1} t_{\text{age},3.5} \gamma_{e,8}^{-1} U_{\text{total},-12}^{-1} \text{ sr}. \end{aligned} \quad (10)$$

The synchrotron and IC emission is given by equations (7) and (8), respectively. The surface brightness of the emission is about  $S = \nu F_\nu / \Omega \sim 1 \times 10^{-8} \theta_{-1}^{-1} E_{n,51} U_{-12} t_{\text{age},3.5}^{-1} \text{ erg s}^{-1} \text{ cm}^{-2} \text{ sr}^{-1}$ .

We may usually assume the emission to be isotropic in the lab-frame, since the Larmor radius is the minimum scale  $r_L < \min(ct_{\text{cool}}, ct_{\text{age}})$  for almost all parameters. For  $\gamma_e \gtrsim 10^{10} \min(2B_{-6}^{1/2} U_{\text{total},-12}^{-1/2}, B_{-6} t_{\text{age},3.5})$ , however, the emission is beamed into the jet direction and the observed flux is reduced.

### 3. Detectability

We calculate now the peak flux and the surface brightness of the emission due to neutrons with a certain Lorentz factor  $\gamma_n$  and total energy  $E_n$ , based on the results of the previous section. A more realistic distribution of neutrons may be described, for our purposes, as a superposition of monoenergetic neutrons. In the following we assume  $E_n = 10^{51}$  erg for  $10^7 \leq \gamma_n < 10^{11}$  and  $E_n = 10^{51}(\gamma_n/10^7)$  erg for  $\gamma_n < 10^7$  as expected in GRBs (Waxman & Bahcall 1997).

Since the emission from the  $\beta$ -decay electrons is extended, it competes with the diffuse background radiation. Since W49B resides in the Galactic disk  $(l, b) = (43.3, -0.2)$ , the disk emission is the main confusion source. In Figure 2 the surface brightness of the disk emission and the  $\beta$ -decay emission are shown. We can see that the IR-optical band (e.g., Bernstein, Freedman, & Madore 2002) and the X-ray band (Kaneda et al. 1997; Snowden et al. 1995) are not suitable for the detection of the  $\beta$ -decay emission considered here,

because the diffuse background dominates. The MeV region (Kinzer, Purcell, & Kurfess 1999; Strong, Moskalenko, & Reimer 2000) could be a possible observing window, but appropriate detectors have not been developed in this band. Although INTEGRAL might be one possibility, the sub-MeV background may be difficult to subtract (Lebrun et al. 2004).

On the other hand, the GeV band (Hunter et al. 1997) and the TeV band appear to be suitable windows for the observation of  $\beta$ -decay IC emission. Strictly speaking, the diffuse background in the TeV band has not been detected. Only an upper limit exists (Aharonian et al. 2001; LeBohec et al. 2000; Amenomori et al. 2002). However the predicted background is below the power-law extrapolation of the upper limit (Aharonian & Atoyan 2000; Strong, Moskalenko, & Reimer 2004), so that it is probable that the TeV background is negligible. Interestingly, one of the upper limits on the TeV background is obtained by the observation of a sky region which includes W49B (Aharonian et al. 2001). The implications of this fact will be discussed below.

We compare now the predicted GeV-TeV flux to the sensitivities of various detectors. Figure 3 shows the flux of the  $\beta$ -decay electrons and the sensitivities of GLAST, HEGRA and VERITAS (e.g., McEnery, Moskalenko, & Ormes 2004). Note that since W49B is in the northern sky, some ground detectors, such as CANGAROO or HESS, are unable to observe it.

It is seen from Figure 3 that GLAST may marginally detect the  $\beta$ -decay emission of W49B. The detectability could be affected by the finite source size, if this is larger than the angular resolution of GLAST. However, the GeV emission comes from neutrons with a Lorentz factor  $\gamma_n \lesssim 10^7$ , so that the emitting region is  $\lesssim 1^\circ \gamma_{n,7}$ , with a shape as shown in Figure 1 (a). Thus, the size of the emission region is comparable to the angular resolution of GLAST,  $3.4^\circ - 0.09^\circ$  (McEnery, Moskalenko, & Ormes 2004).

HEGRA, whose angular resolution is  $\sim 0.1^\circ$ , should take the source size into account. Since the search region in the sky has to be expanded, more background is included. The sensitivity is proportional to the inverse square of the background in the background dominated counting statistics. Therefore the flux sensitivity of an atmospheric Cherenkov telescope to an extended source,  $F_\nu^{\text{extend}}$ , is given by

$$F_\nu^{\text{extend}} = F_\nu^{\text{point}} (\Omega / \pi \theta_{\text{cut}}^2)^{1/2}, \quad (11)$$

where  $F_\nu^{\text{extend}}$  is the sensitivity to a point source, and  $\theta_{\text{cut}} \sim 0.1^\circ$  is the angular cut in the point source analysis (Konopelko, Lucarelli, Lampeitl, & Hofmann 2002; Lessard, Buckley, Connaughton, & Le Bohec 2001). In Figure 3 the dashed lines show the corrected  $\beta$ -decay emission  $\nu F_\nu (\Omega / \pi \theta_{\text{cut}}^2)^{-1/2}$ , which should be compared with the detector sensitivity. We can

see that HEGRA may marginally detect the  $\beta$ -decay emission.

Actually, HEGRA has observed the region including W49B (Aharonian et al. 2001, 2002). An upper limit on the TeV flux from W49B is obtained as  $\sim 0.14$  Club flux  $\sim 7 \times 10^{-12}$  erg cm $^{-2}$  s $^{-1}$  (Aharonian et al. 2002). However this limit constrains the flux only from a  $\sim 0.1^\circ$  circle centered on W49B, since the angular cut  $\theta_{\text{cut}} \sim 0.1^\circ$  is applied in the analysis. Thus the limit is not so crucial. In order to improve the sensitivity to the  $\beta$ -decay emission, we should expand the angular cut  $\theta_{\text{cut}}$  so that all the  $\beta$ -decay emitting region is included in the analysis. The probable size is  $\sim 0.1^\circ \times 1^\circ$ , centered on W49B and with a shape as in Figure 1 (a), possibly along the direction in which more metals are ejected within W49B. Although HEGRA has ended observing, a reanalysis of the data on this region may constrain the  $\beta$ -decay emission.

Whipple is working, but its sensitivity is a few times lower than HEGRA, so that the necessary observation time may be  $\sim 10$  times larger. The future detector VERITAS, following on Whipple, has a  $\sim 10$  times better sensitivity than HEGRA. Therefore, observations by VERITAS would be able to verify or disprove the model.

#### 4. Discussion

The possibility of imaging the  $\beta$ -decay emission region of a GRB remnant could open a novel way of constraining the structure of GRB jets. Currently jets are unresolved, but recent studies indicate that the jet structure is essential to an understanding the GRB phenomenon (Rossi, Lazzati, & Rees 2002; Zhang & Mészáros 2002; Zhang et al. 2004). Depending on the jet structure and the viewing angle, the same jet may be observed as different phenomena, such as short GRBs, long GRBs, X-ray flashes and X-ray rich GRBs (Yamazaki, Ioka, & Nakamura 2004, 2002; Ioka & Nakamura 2001). It is difficult to determine the jet structure from observations of the photon light curve and spectra during the GRB and afterglow phase, because the physical dimensions in these stages are much smaller than the decay lengths considered here, and the relativistic beaming prevents observing the whole angle of the jet. TeV imaging of the  $\beta$ -decay emission could be a possible way<sup>1</sup> to determine or constrain the jet structure, since it provides a much longer lever arm to trace the inner jet.

There are a number of uncertainties which could affect the conclusions. For instance, the photon energy density field may be higher than estimated from the diffuse backgrounds,

---

<sup>1</sup>Other methods might include gravitational waves (Sago, Ioka, Nakamura, & Yamazaki 2004; Kobayashi & Mészáros 2003).

due to contributions from the nearby H II region W49A. The latter emits about  $10^{51}$  Lyman continuum photons  $\text{s}^{-1}$  (Conti & Blum 2002), hence the corresponding photon energy density is  $\sim 10^{-14}(d_A/1 \text{ kpc})^{-2} \text{ erg cm}^{-3}$ , where  $d_A$  is the distance from W49A. Since the projected distance between W49A and W49B is  $\sim 40 \text{ pc}$ , the IC emission within  $\sim 100 \text{ pc}$  of W49B may be enhanced. Also, if the jet is directed towards us, relativistic effects such as a superluminal motion or differential Doppler boosting may be important. However, the barrel shape of W49B possibly suggests that the jet is not directed towards us.

To infer the jet structure precisely, the sky distribution of the electrons must be nearly preserved. Thus the diffusion length of electrons has to be smaller than the emitting region. The diffusion length  $r_D \sim (\kappa t_{\text{age}})^{1/2} \sim 100\gamma_{e,8}^{1/6} t_{\text{age},3.5} \text{ pc}$  within the remnant age  $t_{\text{age}}$  is smaller than the emitting region for  $\gamma_e \sim 10^8$ , if we use the diffusion coefficient of electrons  $\kappa \sim 4 \times 10^{28}(\gamma_e m_e c^2/\text{GeV})^{1/3} \text{ cm}^2 \text{ s}^{-1}$  (Strong, Moskalenko, & Reimer 2004). However we should note that the diffusion coefficient has large uncertainties.

Even if W49B is not a GRB remnant, there may exist other, older GRB remnants, whose age may be  $\lesssim 10^5 \text{ yr}$ , since the (collimation corrected) GRB rate is  $\gtrsim 10^{-5} \text{ yr}^{-1} \text{ galaxy}^{-1}$ . We have replotted Figure 3 in Figure 4, where we replaced the remnant age  $t_{\text{age}}$  by  $10^5 \text{ yr}$ . As long as the electron diffusion length does not become a limiting factor, the  $\beta$ -decay emission from such an older remnant may be detectable.

We thank S. Razzaque, K. Mori and S. Park for useful discussions. This work was supported in part by the Center for Gravitational Wave Physics under the National Science Foundation cooperative agreement PHY 01-14375 (KI, SK), NASA NAG5-13286, NSF AST 0098416 and the Monell Foundation.

## REFERENCES

Aharonian, F. A., & Atoyan, A. M. 2000, A&A, 362, 937  
Aharonian, F. A., et al. 2001, A&A, 375, 1008  
Aharonian, F. A., et al. 2002, A&A, 395, 803  
Amenomori, M., et al. 2002, ApJ, 580, 887  
Bernstein, R. A., Freedman, W. L., & Madore, B. F. 2002, ApJ, 571, 56  
Biermann, P. L., Medina Tanco, G., Engel, R., & Pugliese, G. 2004, ApJ, 604, L29

Bloom, J. S., Frail, D. A., & Kulkarni, S. R. 2003, *ApJ*, 594, 674

Conti, P. S., & Blum, R. D. 2002, *ApJ*, 564, 827

Dermer, C. D. 2002, *ApJ*, 574, 65

Enomoto, R., et al. 2002, *Nature*, 416, 823

Hunter, S. D., et al. 1997, *ApJ*, 481, 205

Ioka, K., & Nakamura, T. 2001, *ApJ*, 554, L163

Kaneda, H., et al. 1997, *ApJ*, 491, 638

Kinzer, R. L., Purcell, W. R., & Kurfess, J. D. 1999, *ApJ*, 515, 215

Kobayashi, S., & Mészáros, P. 2003, *ApJ*, 585, L89

Konopelko, A., Lucarelli, F., Lampeitl, H., & Hofmann, W. 2002, astro-ph/0209431

LeBohec, S., et al. 2000, *ApJ*, 539, 209

Lebrun, F., et al. 2004, *Nature*, 428, 293

Lessard, R. W., Buckley, J. H., Connaughton, V., Le Bohec, S. 2001, *APh*, 15, 1

Mathis, J. S., Mezger, P. G., & Panagia, N. 1983, *A&A*, 128, 212

McEnerly, J. E., Moskalenko, I. V., & Ormes, J. F. 2004, astro-ph/0406250

Milgrom, M., & Usov, V. 1995, *ApJ*, 449, L37

Perna, R., & Loeb, A. 2000, *ApJ*, 533, 658

Rachen, J. P., & Mészáros, P. 1998, *Phys. Rev. D*, 58, 123005

Rossi, E., Lazzati, D., & Rees, M. J. 2002, *MNRAS*, 332, 945

Sago, N., Ioka, K., Nakamura, T., & Yamazaki, R. 2004, astro-ph/0405067

Snowden, S. L. 1995, *ApJ*, 454, 643

Strong, A. W., Moskalenko, I. V., & Reimer, O. 2000, *ApJ*, 537, 763

Strong, A. W., Moskalenko, I. V., & Reimer, O. 2004, *ApJ* in press, astro-ph/0406254

Vietri, M. 1995, *ApJ*, 453, 883

Vietri, M. 1998, Phys. Rev. Lett., 80, 3690

Vietri, M., De Marco, D., & Guetta, D. 2003, ApJ, 592, 378

Waxman, E. 1995, Phys. Rev. Lett., 75, 386

Waxman, E. 2004, ApJ, 606, 988

Waxman, E., & Bahcall, J. 1997, Phys. Rev. Lett., 78, 2292

Yamazaki, R., Ioka, K., & Nakamura, T. 2002, ApJ, 571, L31

Yamazaki, R., Ioka, K., & Nakamura, T. 2004, ApJ, 607, L103

Zhang, B., & Mészáros, P. 2002, ApJ, 571, 876

Zhang, B., Dai, X. Y., Lloyd-Ronning, N. M., & Mészáros, P. 2004, ApJ, 601, L119

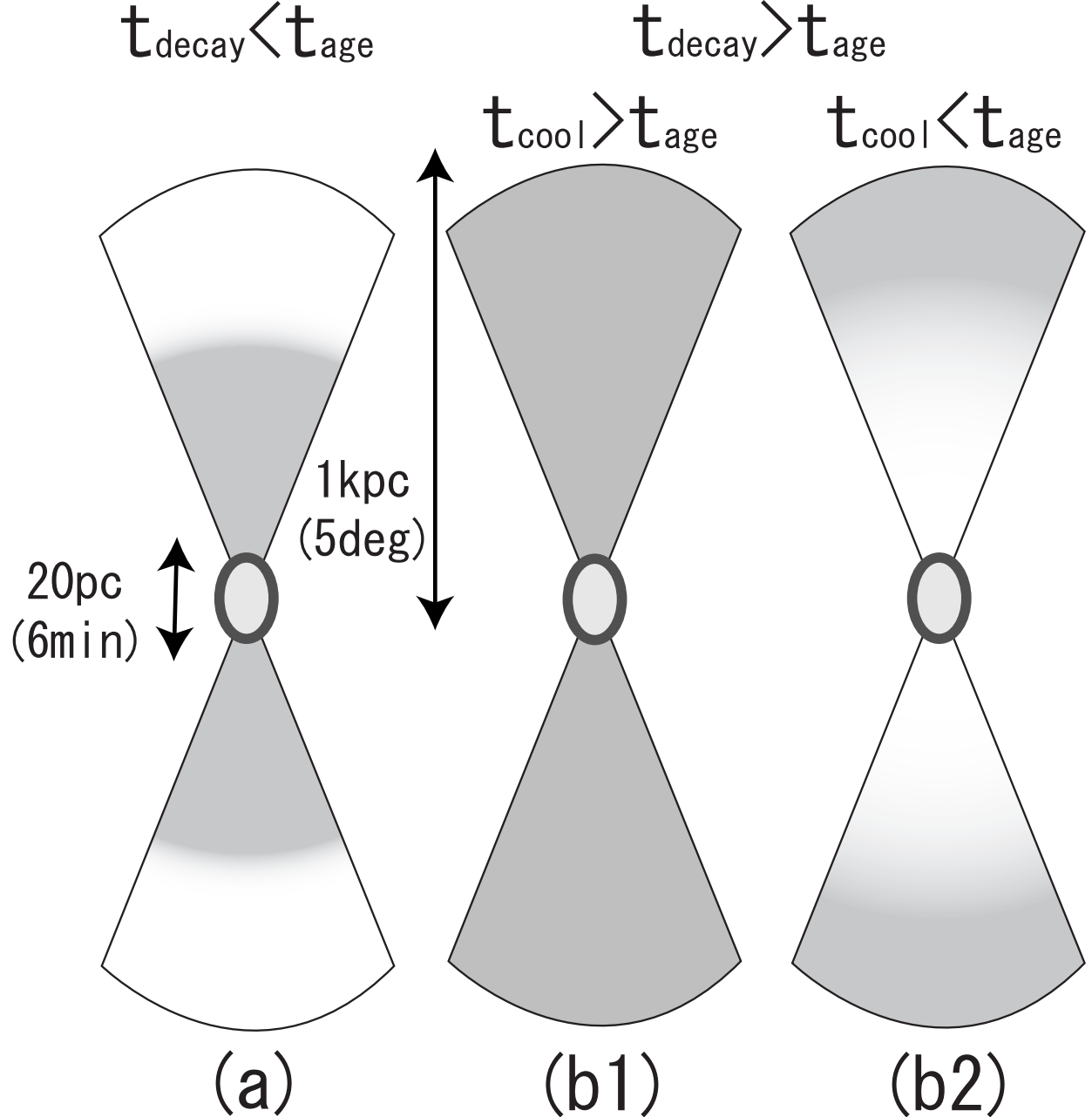


Fig. 1.— The GeV-TeV emission region (shaded region) on the sky is shown schematically. (a) The  $\beta$ -decay time is shorter than the remnant age  $t_{\text{decay}}(\gamma_e) < t_{\text{age}}$ , so that the radius of the emitting region is about the  $\beta$ -decay length in equation (2). The surface brightness on the sky is nearly homogeneous. (b1)  $t_{\text{decay}}(\gamma_e) > t_{\text{age}}$  and the initial cooling time is longer than the remnant age  $t_{\text{cool}}(\gamma_e) > t_{\text{age}}$ . The radius of the emitting region is about  $\sim ct_{\text{age}} \sim 1t_{\text{age},3.5}$  kpc. The surface brightness is nearly homogeneous. (b2)  $t_{\text{decay}}(\gamma_e) > t_{\text{age}}$  and  $t_{\text{cool}}(\gamma_e) < t_{\text{age}}$ . The radius of the emitting region is about  $\sim ct_{\text{age}} \sim 1t_{\text{age},3.5}$  kpc. The jet head region, of size  $\sim ct_{\text{cool}}(\gamma_e)$ , has a flux  $\sim t_{\text{age}}/t_{\text{cool}}$  times larger than the rest. The GRB remnant W49B, shown in the center, has a radius  $\sim 10$  pc.

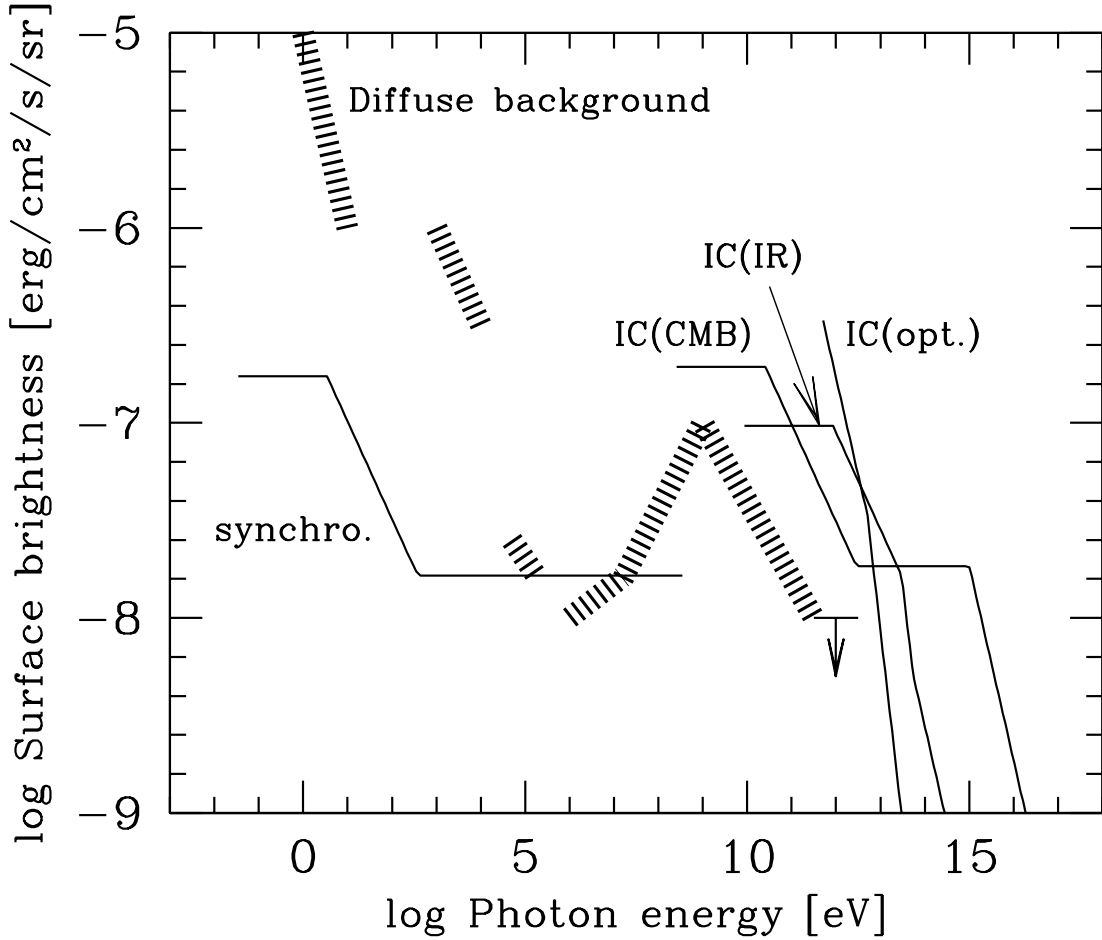


Fig. 2.— The surface brightness of the emission from  $\beta$ -decay electrons due to synchrotron and inverse Compton (IC) on background photons is shown as solid lines, compared with that of the diffuse background radiation (hashed lines). Shown are the IR-optical background (Bernstein, Freedman, & Madore 2002), the X-ray background (Kaneda et al. 1997; Snowden et al. 1995), the MeV background (Kinzer, Purcell, & Kurfess 1999; Strong, Moskalenko, & Reimer 2000), the GeV background (Hunter et al. 1997), and an upper limit on the TeV background (Aharonian et al. 2001; LeBohec et al. 2000; Amenomori et al. 2002). The diffuse background dominates the  $\beta$ -decay emission in the IR-optical and X-ray band.

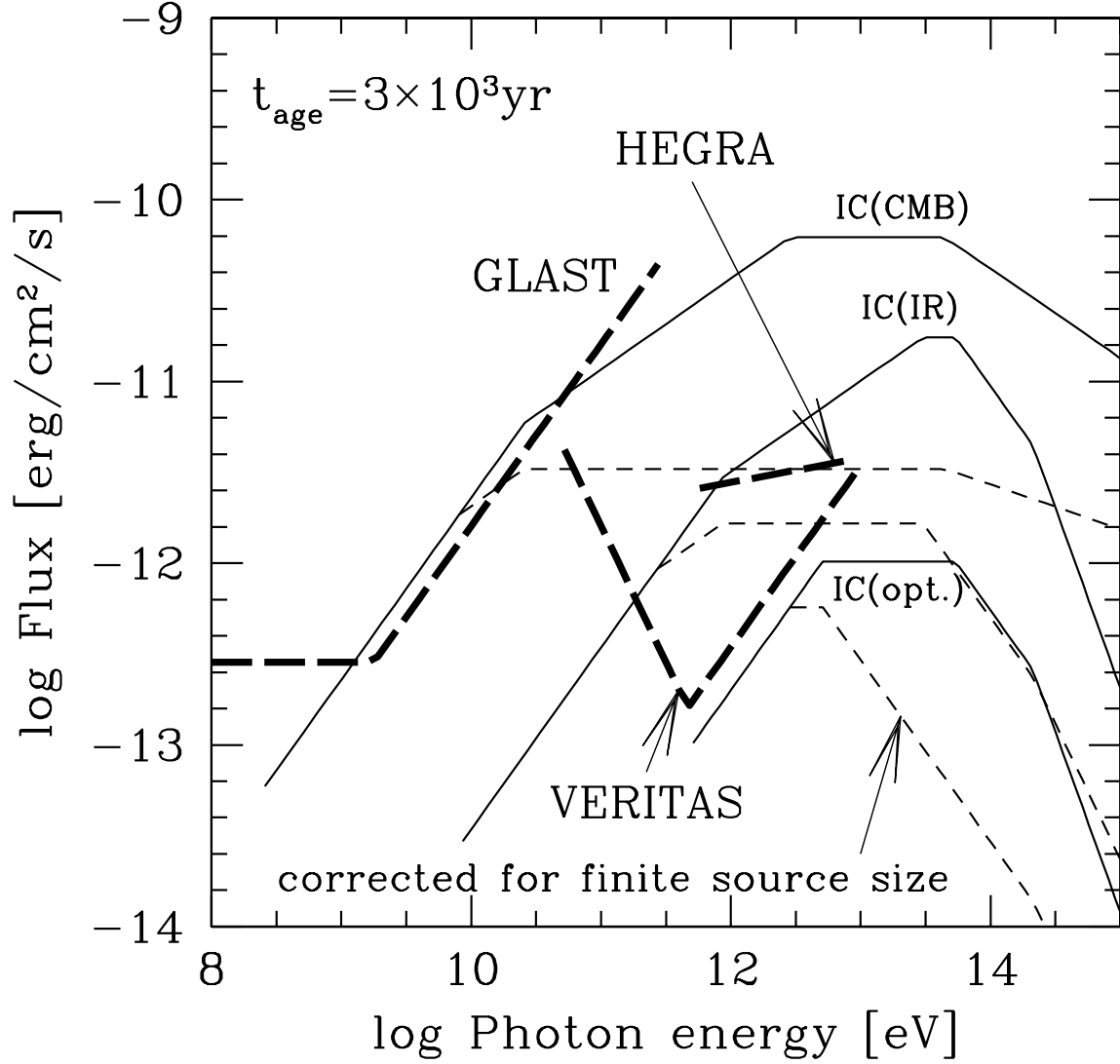


Fig. 3.— The flux of emission from the  $\beta$ -decay electrons is compared with the detector sensitivity. The solid lines show the IC fluxes of the CMB, IR and optical photons. The bold long dashed lines are the sensitivities of GLAST, HEGRA and VERITAS (e.g, McEnery, Moskalenko, & Ormes 2004). The dashed lines are the flux of  $\beta$ -decay emission multiplied by  $(\Omega/\pi\theta_{\text{cut}})^{-1/2}$  in order to take the finite source size into account, where  $\Omega$  is the solid angle of the emitting region on the sky and  $\theta_{\text{cut}} \sim 0.1^\circ$  is the angular cut in the analysis. The sensitivities of HEGRA and VERITAS should be compared with the dashed lines. The remnant age is  $t_{\text{age}} = 3 \times 10^3$  yr.

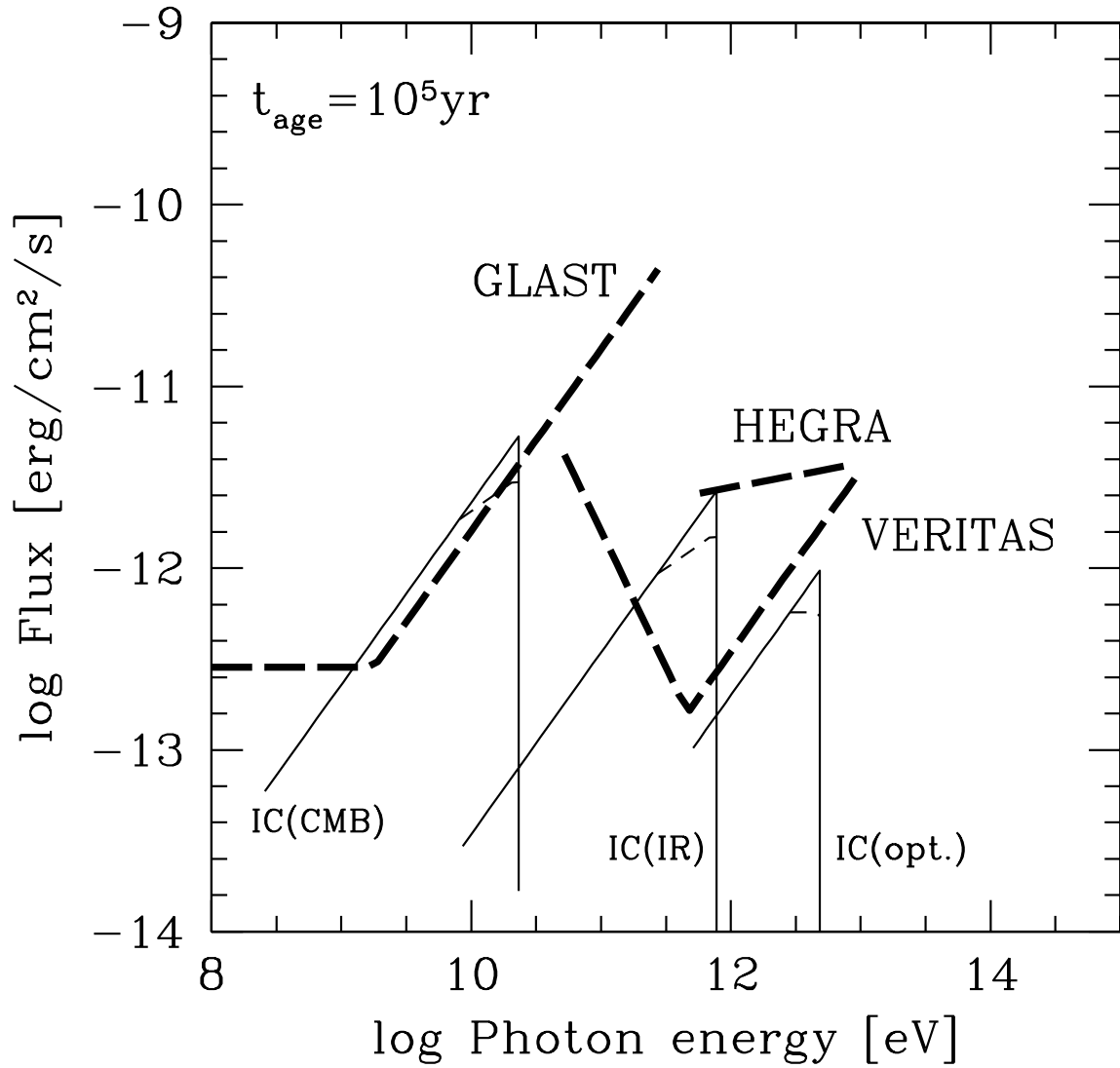


Fig. 4.— Same as Figure 3 except for the remnant age, which is taken here as  $t_{\text{age}} = 10^5 \text{ yr}$ .